

University of Texas Rio Grande Valley

**ScholarWorks @ UTRGV**

---

Theses and Dissertations - UTB/UTPA

---

8-2006

## Image up-sampling using the discrete wavelet transform

Laleh Asgharian

*University of Texas-Pan American*

Follow this and additional works at: [https://scholarworks.utrgv.edu/leg\\_etd](https://scholarworks.utrgv.edu/leg_etd)



Part of the [Computer Sciences Commons](#)

---

### Recommended Citation

Asgharian, Laleh, "Image up-sampling using the discrete wavelet transform" (2006). *Theses and Dissertations - UTB/UTPA*. 740.

[https://scholarworks.utrgv.edu/leg\\_etd/740](https://scholarworks.utrgv.edu/leg_etd/740)

This Thesis is brought to you for free and open access by ScholarWorks @ UTRGV. It has been accepted for inclusion in Theses and Dissertations - UTB/UTPA by an authorized administrator of ScholarWorks @ UTRGV. For more information, please contact [justin.white@utrgv.edu](mailto:justin.white@utrgv.edu), [william.flores01@utrgv.edu](mailto:william.flores01@utrgv.edu).

IMAGE UP-SAMPLING USING THE  
DISCRETE WAVELET TRANSFORM

A Thesis

By

Laleh Asgharian

Submitted to the Graduate School of the  
University of Texas-Pan American  
In partial fulfillment of the requirements for the degree of  
MASTER OF SCIENCE

August 2006

Major Subject: Computer Science

IMAGE UP-SAMPLING USING THE  
DISCRETE WAVELET TRANSFORM

A Thesis  
by  
LALEH ASGHARIAN

Approved as to style and content by:



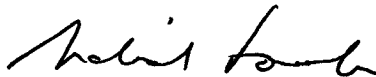
---

Dr. Ping-Sing Tsai  
Chair of Committee



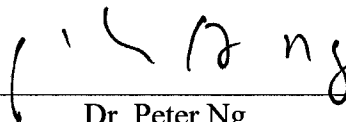
---

Dr. Zhixiang Chen  
Committee Member



---

Dr. Richard Fowler  
Committee Member



---

Dr. Peter Ng  
Committee Member

August 2006

## ABSTRACT

Asgharian, Laleh, Image Up-Sampling Using the Discrete Wavelet Transform. Master of Science (MS), August, 2006, 43 pp., 3 tables, 12 illustrations, 24 references, 14 titles.

Image up-sampling is an effective technique, useful in today's digital image processing applications and rendering devices. In image up-sampling, an image is enhanced from a lower resolution to a higher resolution with the degree of enhancement depending upon application requirements. It is known that the traditional interpolation based approaches for up-sampling, such as the Bilinear or Bicubic interpolations, blur the resultant images along edges and image features. Furthermore, in color imagery, these interpolation-based up-sampling methods may have color infringing artifacts in the areas where the images contain sharp edges and fine textures. We present an interesting up-sampling algorithm based on the Discrete Wavelet Transform (DWT). The proposed method preserves much of the sharp edge features in the image, and lessens the amount of color artifacts. Effectiveness of the proposed algorithm has been demonstrated based on comparison of PSNR and  $\Delta E_{ab}^*$  quality metrics between the original and reconstructed images.

## ACKNOWLEDGEMENTS

I would like to thank the members of my thesis committee, Professors Zhixiang Chen, Richard Fowler, Peter Ng, and Ping-Sing Tsai for agreeing to take the time to serve on this committee. I also want to thank my husband, Dr. Heinrich Foltz for his invaluable help and advice in all aspects of this work.

Above all, I am most deeply indebted to my supervising professor for his ideas, guidance, support, and tremendous help, in making this work possible. I will always take pride in saying that I studied under, and worked with, Professor Ping-Sing Tsai.

## TABLE OF CONTENTS

	Page
ABSTRACT.....	iii
ACKNOWLEDGEMENTS.....	iv
TABLE OF CONTENTS.....	v
LIST OF TABLES.....	vii
LIST OF FIGURES.....	viii
CHAPTER I. INTRODUCTION AND RELATED WORKS.....	1
A. Conceptual Framework of the DWT.....	2
B. Literature Review of Image Interpolation.....	9
CHAPTER II. DWT BASED IMAGE UP-SAMPLING.....	13
A. Proposed Methodology.....	13
B. Implementations.....	16
C. Selection of Scaling Factor.....	17
CHAPTER III. EXPERIMENTAL RESULTS.....	19
A. Image Quality Metrics.....	19
B. Results Using Different DWT Implementations and Filters.....	24
C. Results for Image Fidelity.....	32
D. Results for Recursive Up-Sampling.....	35
E. Results for Combination of Bicubic and DWT.....	36

CHAPTER IV. CONCLUSION.....	38
REFERENCES.....	40
VITA.....	43

## LIST OF TABLES

Table I. PSNR AND $\Delta E_{ab}^*$ COMPARISONS.....	31
Table II: IMAGE FIDELITY COMPARISON RESULTS.....	34
Table III: PSNR COMPARISONS FOR IMAGE MULTIPLIED BY A FACTOR OF THREE.....	37

## LIST OF FIGURES

Figure 1: Signal analysis and reconstruction in 1D DWT .....	5
Figure 2: Signal analysis and reconstruction in two-level 1D DWT.....	6
Figure 3: Three levels of decomposition in 2D DWT.....	7
Figure 4: Example of LL, HL, LH, and HH subbands generated from a real image <i>I</i> . (a) original BIKE Image and subbands; (b) after level 1 (c) after level 2 (d) after level 3 decomposition. ....	8
Figure 5: DWT based image up-sampling.....	15
Figure 6: Original test images used in the experiment.....	20
Figure 7: Up-sampling results with proposed DWT based approach using 9/7 filters.....	26
Figure 8: Up-sampling results with proposed DWT based approach using 5/3 filters.....	27
Figure 9: Experimental results for ZEBRA image.....	28
Figure 10: Experimental results for STAR image.....	29
Figure 11: (a) Homogeneity image of ZEBRA green channel. (b) Blended mask image of RGB channels.....	32
Figure 12: Experimental results for recursive up-sampling.....	36

## CHAPTER I

### INTRODUCTION AND RELATED WORKS

The Discrete Wavelet Transform (DWT) [1] has become a versatile tool in modern digital image processing applications such as pattern recognition, image enhancement [2], image compression [3], image interpolation [4], etc. Image interpolation techniques have been developed to transform an image from one resolution to another [4, 5, 6]. When an image is interpolated from a higher resolution to a lower resolution, it is traditionally called image downscaling or down-sampling. On the other hand, when an image is interpolated from a lower resolution to a higher resolution, it is referred as image up-scaling or up-sampling.

In this thesis, we propose a novel image interpolation technique using the Discrete Wavelet Transform. This method is intended to allow magnification of an image to any desired size with enhanced image quality compared to traditional up-sampling methods as measured by objective quality metrics and subjective impression.

#### *A. Conceptual Framework of the Discrete Wavelet Transform*

The wavelet transform, introduced in the late 1950s is based on small waves or “wavelets” containing both frequency and temporal information, with the energy of the

wavelets concentrated in time. Unlike in Fourier representation of signals in which signals are time-invariant and periodic, providing only frequency information, wavelets allow both time and frequency analysis of transient, time-variant signals. To analyze the information content of images, Mallat proposed the theory of “multi-resolution decomposition” of signals in 1989 using wavelets in time-scale space, with a *pyramidal algorithm* based on convolutions with quadrature mirror filters [1].

Multi-resolution decomposition allows us to study the image detail at different resolutions, emphasizing different image structures at each resolution, as we typically move from coarser to finer resolution. Keep in mind that the coarser image features represent the “context” information in the image, and that each resolution level, a different set of details become apparent and conspicuous.

Let us first briefly describe a wavelet. Wavelets are functions obtained from a single prototype or basis function by dilations (or scaling) and translations (or shifting) in the time (or frequency) domain as shown:

$$\psi_{a,b}(t) = \frac{1}{\sqrt{a}} \psi\left(\frac{t-b}{a}\right)$$

where  $a$  is the scaling parameter and  $b$  is the shifting parameter. The 1-D wavelet transform is given by:

$$W(a,b) = \int_{-\infty}^{\infty} x(t) \psi_{a,b}(t) dt$$

where  $x(t)$  represents the signal function. The inverse 1-D wavelet transform is given by:

$$x(t) = \frac{1}{C} \int_{a=-\infty}^{\infty} \int_{b=-\infty}^{\infty} \frac{1}{|a|^2} W(a,b) \psi_{a,b}(t) da db,$$

where

$$C = \int_{-\infty}^{\infty} \frac{|\psi(\omega)|^2}{|\omega|} d\omega,$$

and  $\psi(\omega)$  is the Fourier transform of the mother wavelet  $\psi(t)$  [3].

A wavelet transform is similar to a Fourier transform in that it involves an integral of the product of the signal and the wavelet function. The difference between a continuous wavelet transform and a discrete wavelet transform is both in the nature of the signal function itself, as well as the dilation and translation parameters which are discrete rather than continuous. Since we are interested in discrete signals, from now on our discussion entails only discrete rather than continuous wavelet transforms.

After Mallat's introduction of multi-resolution decomposition of signals, the discrete wavelet transform (DWT) became a very popular tool for signal processing applications. In this technique, a signal is represented using a collection of coefficients, providing information about both the position and frequency of the signal. This method has an advantage over the Fourier transform and other methods in that it produces localization in both the time and frequency domains. Consequently, the DWT decomposes a signal into different subbands such that the lower frequency subbands have coarser time resolution and finer frequency resolution than the higher frequency subbands, such that the quality of the image depends on the level of resolution. Its versatility and its support of progressive image transmission and region of interest coding are some of the reasons for its use today in the JPEG2000 image compression standard.

Recall that in multi-resolution analysis [1], the goal is to represent a function  $x(t)$  using approximations at different levels of resolution. In the pyramidal algorithm, the resolution step is chosen to be equal to 2. Then, a wavelet orthonormal basis is used to

decompose the function using the difference in information between the approximation at resolution  $2^{j+1}$  and that at approximation  $2^j$ , in other words the detail signal at the resolution  $2^j$ . We can consider the wavelet coefficients as providing the detail information going from a coarser to a finer resolution. At each decomposition level the signal can be decomposed into two parts, one representing the coarse approximation of the signal at a lower resolution, and the other the detail information, lost in the approximation process.

The DWT can be implemented by filtering operations with well-defined filter coefficients [7]. In the traditional convolution (filtering) based approach for computation of the forward DWT, the input signal ( $x$ ) is filtered separately by a low-pass filter ( $\tilde{h}$ ) and a high-pass filter ( $\tilde{g}$ ). The two output streams are then sub-sampled by simply dropping the alternate output samples in each stream to produce the low-pass ( $y_L$ ) and high-pass ( $y_H$ ) subband outputs as shown in Fig. 1. The two filters ( $\tilde{h}$ ,  $\tilde{g}$ ) form the *analysis* filter bank. The original signal can be reconstructed by a *synthesis* filter bank ( $h$ ,  $g$ ) starting from  $y_L$  and  $y_H$  as shown in Fig. 1. Given a discrete signal  $x(n)$ , the output signals  $y_L(n)$  and  $y_H(n)$  in Fig. 1 can be computed as follows:

$$y_L(n) = \sum_{i=0}^{\tau_L-1} \tilde{h}(i)x(2n-i),$$

$$y_H(n) = \sum_{i=0}^{\tau_H-1} \tilde{g}(i)x(2n-i)$$

where  $\tau_L$  and  $\tau_H$  are the lengths of the low-pass( $\tilde{h}$ ) and high-pass ( $\tilde{g}$ ) filters respectively. During the inverse transform computation, both  $y_L$  and  $y_H$  are first up-

sampled by inserting zeros in between each pair of samples and then filtered by the low-pass ( $h$ ) and high-pass ( $g$ ) filters respectively. Then they are added together to obtain the reconstructed signal ( $x'$ ) as shown in Fig. 1.

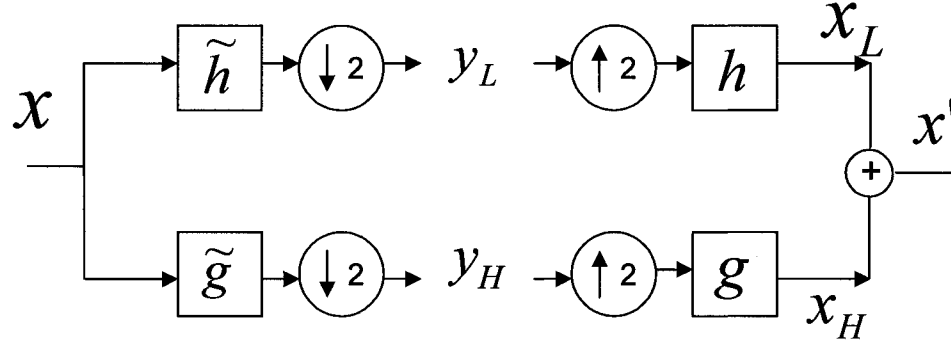


Figure 1: Signal analysis and reconstruction in 1D DWT.

For multi-resolution wavelet decomposition, the low-pass subband ( $y_L$ ) is further decomposed in a similar fashion in order to get the second-level of decomposition, and the process is repeated. The inverse process follows similar multi-level synthesis filtering in order to reconstruct the signal. A two level DWT decomposition and its reconstruction have been shown in Fig. 2, as an example. Image signals are two-dimensional signals. As a result, we need to apply two-dimensional DWT on image signals for digital image processing applications. Since two dimensional wavelet filters are separable functions, the two-dimensional DWT can be implemented by first applying the one-dimensional DWT row-wise to produce an intermediate result (L and H subbands in each row) and then applying the same one-dimensional DWT column-wise on the intermediate result to produce the final result (known as wavelet coefficients), as shown in Fig. 3(a). In the first level of decomposition, four subbands LL1, LH1, HL1 and HH1 are obtained. Repeating the same process to the LL1 subband, it produces LL2, LH2, HL2 and HH2 and so on, as

shown in Fig. 3(b)-(c).

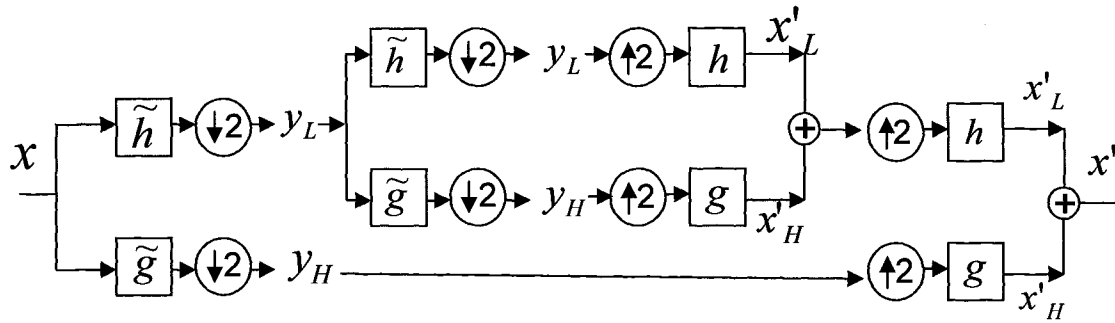
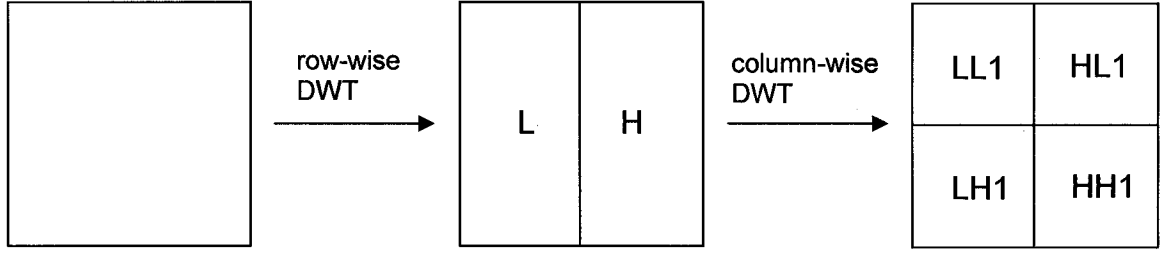
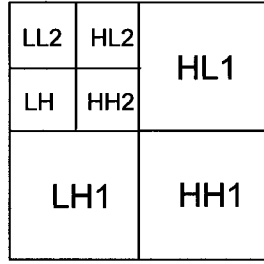


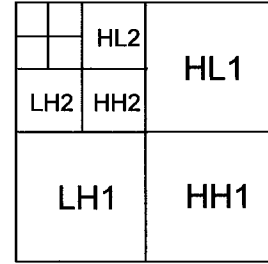
Figure 2: Signal analysis and reconstruction in two-level 1D DWT.



(a) First level of decomposition



(b) Second level of decomposition



(c) Third level of decomposition

Figure 3: Three levels of decomposition in 2D DWT.

As shown in Fig. 4(b), four subbands  $LL$ ,  $HL$ ,  $LH$ , and  $HH$  are generated after applying one level of DWT in the input image  $I$  (one of the ISO/IEC test images, BIKE, provided by the JPEG2000 standard committee). It is interesting to note that the  $LL$  subband can be used as a 2:1 downsampled version of the original image after properly normalizing each sample in the  $LL$  subband. The basic idea behind the application of DWT for image interpolation to up-sample an image is to modify all the wavelet subbands to a higher resolution by a suitable method which we will discuss in the following sections and then inverse transform (IDWT) it to obtain the interpolated image as explained schematically in Chapter II.A.(Fig. 5).

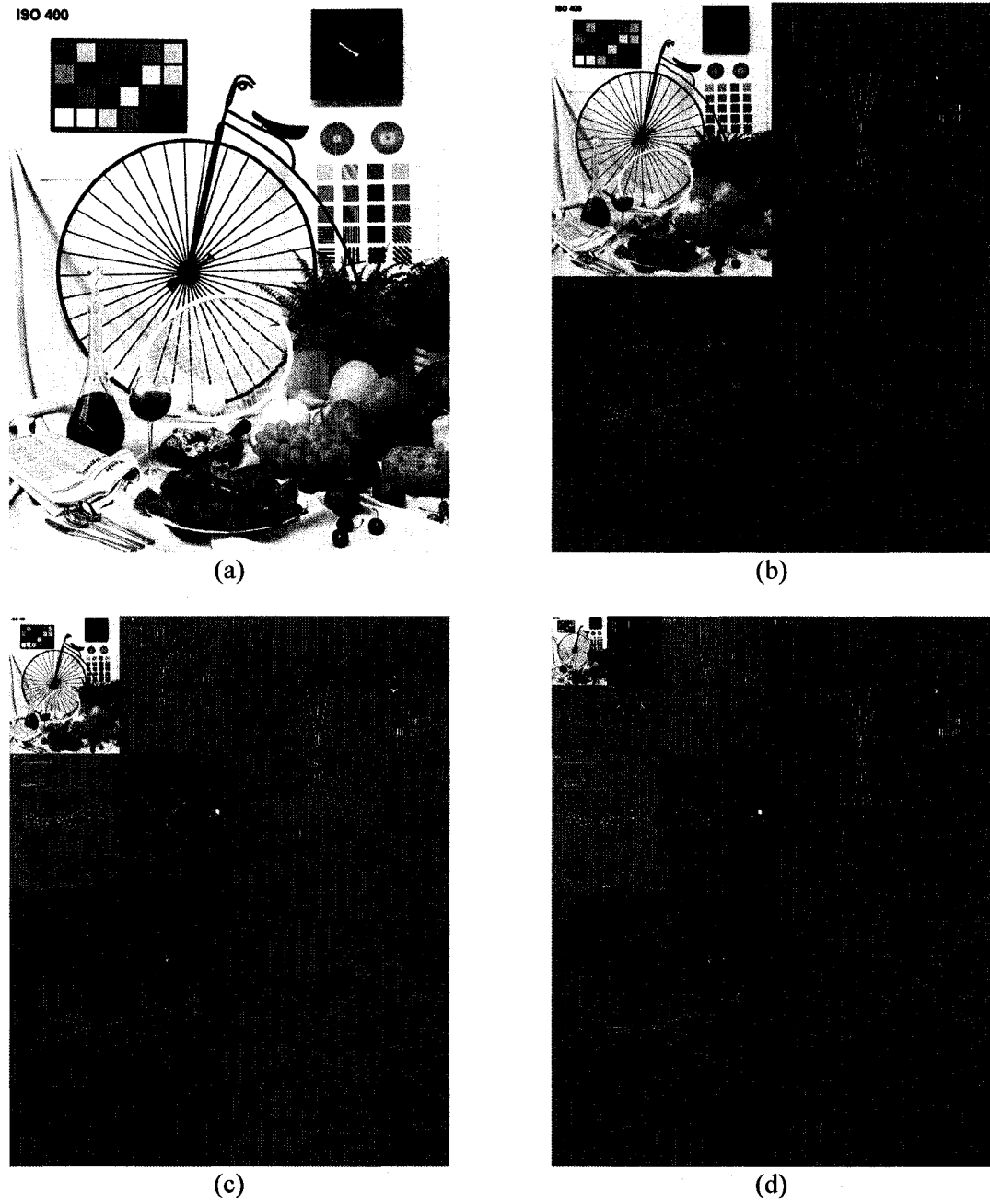


Figure 4: Example of LL, HL, LH, and HH subbands generated from a real image  $I$ . (a) Original BIKE image and subbands; (b) after level 1, (c) after level 2, (d) after level 3 decomposition.

### *B. Literature Review of Image Interpolation*

In image interpolation, an image is transformed from one resolution to a different resolution. Interpolation techniques can be adaptive or non-adaptive in nature. The popularly used simple non-adaptive image interpolation techniques are bilinear interpolation, bicubic interpolation, and nearest-neighbor replacement and used in the commercial image processing tools such as Adobe® Photoshop® CS2 software [9]. Bilinear interpolation can be considered as a weighted average of four neighboring points. The intensity of the point of interest is estimated to be bilinear in this neighborhood. Bicubic interpolation uses sixteen neighboring points for estimation. It approximates the local intensity values using a bicubic polynomial surface. There are several adaptive techniques proposed in the literature [10, 11, 12, 13].

The method proposed by Hong, *et al.* [10] known as “directional interpolation” overcomes common problems associated with standard interpolation techniques, such as image blurring and blocking artifacts, resulting in more natural looking magnified images in applications like the camcorder zoom. They accomplish this by retaining the sharpness of edges appearing in the image in different arbitrary directions. Local edge information in the image is extracted using DCT coefficients, which are also used to specify one of five different edge types. The edge type then helps specify the interpolation method that is to be applied to the local region. Then, Cubic B-Spline Transformation is applied, followed by a combination of zero order and bilinear interpolations. Finally, five different Gaussian low-pass filters are applied to reduce the discontinuities and blocking artifacts generated by the interpolation procedure.

Li, *et al.* [11] use a multi-resolution “edge-directed covariance based adaptation

method” to statistically model the interpolation to any arbitrary edge orientation so that, unlike Hong *et al.*’s approach, they need not restrict themselves to specific edge orientations. However, since this technique is computationally quite expensive, they only apply it to “edge pixels” and for other regions of the image, “non-edge pixels”, they apply the usual bilinear interpolation method, since edge pixels only cover a small fraction (5-15%) of the image. They then test their algorithm to enhance the resolution of a grayscale image and to reconstruct a full-resolution color image from CCD (charge-coupled device) samples and demonstrate enhanced quality over linear interpolation in both applications using subjective perceptual measures. First, the image is modeled as a locally stationary Gaussian process. Then, the high resolution covariance is estimated from its low-resolution version using “geometric duality”, that is, the relation between pixels at different resolutions that lie along the same orientation without use of explicit information about edge orientation. The low-resolution covariance is estimated from the four nearest diagonal neighbors. Finally, the high-resolution covariance estimate is used to obtain the minimum mean square error linear interpolation coefficients using Wiener filtering theory. The major disadvantage of this method, which is the computational complexity, can be reduced by applying it only to edge pixels, which make up only a small fraction of the whole image.

Hwang, *et al.*’s approach [12] uses local gradient information to adapt the bilinear and bicubic interpolation algorithms to yield better perceptual image quality and improved image metrics like the PSNR value. In addition they are able to overcome problems such as the smoothing of edges that conventional interpolation algorithms have not yet resolved. They then test their two adaptive “inverse gradient” interpolation algorithms on

a set of six test images and demonstrate enhanced preservation of structural features and edge regions. In this method, the weights of the input image pixels, which in conventional interpolation algorithms are functions of distance only, are modified by dividing by the normalized local gradients to yield a better interpolation estimate when the gradient changes abruptly as in edge regions and across image features.

Carrato, *et al.* [13] introduce a rational interpolator, providing a nonlinear interpolation procedure that produces sharp synthetic and natural images with minimum blurring and undesirable artifacts. First, each pixel to be interpolated is divided into quarters. Then a subset of a  $3 \times 3$  pixel mask is used to make corrections to the value of the pixel where the edges may be either sharp or smooth. The correction is made by taking appropriate weights of all the possible difference pixels (pairs) and averages of difference pixels using some optimization procedure. To ensure that both sharp and smooth edges are accurately interpolated, the operator should be height independent, reducing the number of possible pattern combinations to consider. With the designation of the interpolator output for all the patterns, the set of parameters are obtained using an optimization process to minimize the mean square error of the interpolator output with respect to the desired pixel value. The authors find that when this procedure is applied to both synthetic and natural images, superior images are produced compared to both the bilinear and bicubic interpolations, yielding sharp, artifact-free images.

The adaptive techniques reviewed in the papers mentioned above usually take into consideration some image content related features such as edges, local gradients, and the like. These techniques are usually computationally more expensive compared to the above non-adaptive techniques. In this thesis, we present a novel DWT based image

interpolation algorithm which is adaptive in nature by virtue of the characteristics of the DWT which divides the image into low and high frequency subbands. The directional edge information (vertical, horizontal, and diagonal) in the image is embedded into the high frequency subbands after wavelet decomposition. The choice of wavelet filters can be determined by a user depending upon the characteristics of the image. However, the underlying operations in the algorithm are not image content dependent and hence non-adaptive in nature. The experimental results are found to be superior compared to the state-of-the-art in the literature.

The remainder of this thesis is organized as follows. Chapter II presents the proposed algorithm and its implementation including a discussion of the scaling factor used in the wavelet filters. Our experimental results are presented in Chapter III. Chapter IV presents the conclusion of our work.

## CHAPTER II

### DWT BASED IMAGE UP-SAMPLING

#### *A. Proposed Methodology*

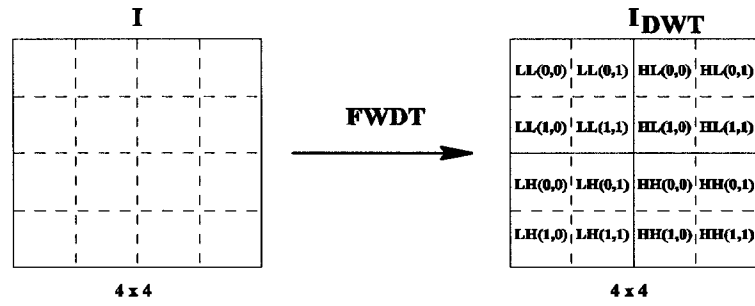
We explain the proposed up-sampling technique with an example, as shown in Fig. 5. We would like to up-sample an input image ( $I$ ) of resolution  $m \times n$  (say  $4 \times 4$  as in Fig. 5) to an image ( $I'$ ) of resolution  $2m \times 2n$ . In the first step, we transform the image using the forward discrete wavelet transform (FDWT) in order to decompose it into four subbands – one low frequency subband ( $LL$ ) and three high frequency subbands ( $HL$ ,  $LH$  and  $HH$ ), resulting in the wavelet coefficient image  $I_{DWT}$  of size  $m \times n$ . These four subbands contain different information about the image. The  $HL$  and  $LH$  subbands contain edge information in different directions, which will be used for the purpose of enhancement in the next step. The  $HH$  subband can be considered as high frequency noise present in the image and can be abandoned to reduce the computational time.

The second step is to form a new wavelet coefficient image  $I'_{DWT}$  of size  $2m \times 2n$ . We call it a virtual DWT image, whose  $LL$  subband is the original input image  $I$  with each pixel multiplied by a *scaling factor*  $s$ . This scaling factor is determined by the DC gain of the low pass filter coefficients used in the DWT, as will be explained in Chapter II.C. Hence, the dimension of the new  $LL$  subband is the same as the resolution  $m \times n$  of the original image  $I$ . The  $HH$  subband of the virtual DWT image ( $I'_{DWT}$ ) is considered to

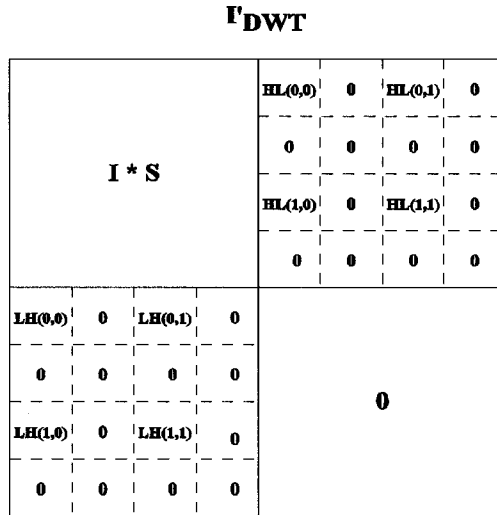
contain all zeros and hence it is nothing but a matrix of zeros with dimension  $m \times n$ . The new  $HL$  and  $LH$  subbands of the virtual DWT image are generated from the original  $HL$  and  $LH$  subbands (computed in the first step) by inserting zeros in alternate rows and columns as shown in Fig. 5(b).

In the last step, we inverse transform (IDWT) this virtual DWT image ( $I'_{DWT}$ ) that we formed in the second step as explained above. The resulting image after IDWT is the desired up-sampled image  $I'$  of resolution  $2m \times 2n$ .

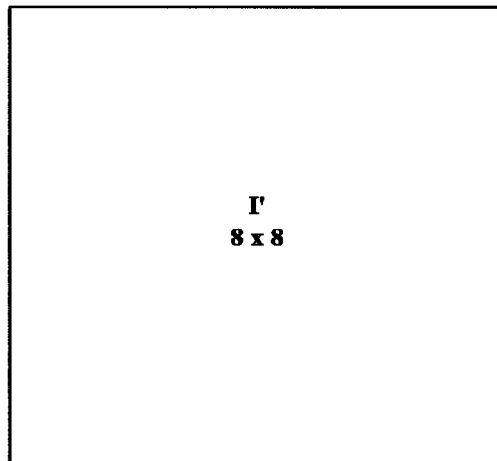
To up-sample color images, the proposed technique can be applied independently in each color plane.



(a)



(b)



(c)

Figure 5: DWT based image up-sampling.

### B. Implementations

The algorithm can be implemented in different ways. Since the 2-D discrete wavelet transform is computed by applying the 1-D low-pass and high-pass filters in succession to the rows and the columns of the input image, and the filtering operation is simply a multiply-and-accumulate operation, the proposed algorithm can be easily implemented in any DWT based hardware architecture or by using a DSP (digital signal processor). The  $HL$  subband of the  $I'_{DWT}$  can be obtained by applying the 1-D high-pass filter row-wise, followed by the 1-D low-pass filter column wise on the input image  $I$ , and then setting the alternate row and column coefficients to zeros. The  $LH$  subband of the  $I'_{DWT}$  can be obtained in a similar fashion by switching the order of applying the high- and low-pass filters.

Alternatively, for software implementation, the proposed up-sampling method can be summarized in the following steps:

1. Initialize a matrix  $I'_{DWT}$  of dimensions  $2m \times 2n$  with all its elements as zeros.
2. Set the original image to a matrix  $I$  of dimension  $m \times n$ .
3. Multiply  $I$  by the scale factor  $s$  to produce a matrix  $I_{LL}$ . Replace the top-left quadrant of  $I'_{DWT}$  by  $I_{LL}$ . The scale factor  $s$  is equal to the square of the DC gain of the selected analysis low-pass filter.
4. Apply the high-pass wavelet filter (without down-sampling) to each row of  $I$  followed by the low-pass filter to each column. Set the alternate rows and columns of the resulting matrix to zeros to produce a matrix  $I_{HL}$ . Replace the top-right quadrant of the matrix  $I'_{DWT}$  by this  $I_{HL}$ .
5. Apply the low-pass wavelet filter (without down-sampling) to each row of  $I$

followed by the high-pass filter to each column. Set the alternate rows and columns of the resulting matrix to zeros to produce a matrix  $I_{LH}$ . Replace the bottom-left quadrant of matrix  $I'_{DWT}$  by this  $I_{LH}$ .

6. Apply the inverse DWT on matrix  $I'_{DWT}$  to produce  $I'$ .

### *C. Selection of Scaling Factor*

Here we discuss the scaling factors associated with the wavelet coefficients so that users can adaptively choose the wavelet filters suitable for particular applications and image characteristics.

The scaling factor  $s$  is set equal to the square of the DC gain of the selected analysis low-pass filter. For a given  $n$ -taps analysis low-pass filter,  $\tilde{h}(n)$ , the expression  $|\sum_n \tilde{h}(n)|$  denotes the DC gain; while  $|\sum_n (-1)^n \tilde{g}(n)|$  denotes the Nyquist gain of a  $n$ -tap analysis high-pass filter,  $\tilde{g}(n)$ . Depending upon the implementation of the discrete wavelet transform, one may choose a different DC gain for the analysis low-pass filter and Nyquist gain for the analysis high-pass filter, or even choose different filters. For more detailed discussion, the readers are referred to the course notes by M. Rabbani and D. Santa-Cruz [14]. In this paper, we first choose the 9/7 bi-orthogonal Spline filters due to the fact that it is commonly used in the literature, and it is one of two default filters used in the JPEG2000 image compression standard [3, 15]. It is known to produce better perceptual quality. We also normalized the 9/7 filters with both the DC and Nyquist gains equal to  $\sqrt{2}$ . This will maintain the same dynamic range for all four subbands. Consequently, the scaling factor,  $s$ , used in the proposed algorithm should be **2**, since that

is the square of the DC gain.

The same theory applies to all other wavelet filters and users can use any other wavelet filter for the proposed image up-sampling technique.

## CHAPTER III

### EXPERIMENTAL RESULTS

In order to demonstrate the proposed merits of the up-sampling method, we have used a large set of color images with different image sizes, shown in Fig. 6 for testing purposes. The test set here includes two large-sized images (Balloon and Flag), four natural mid-sized images from Kodak Photo CD [16] (Hat, Parrots, Sails and Lighthouse), and two small-sized images (Star and Zebra) with a lot of edge content. The test images are first down-sampled by a factor of two in both the vertical and horizontal directions. A simple sub-sampling method is used to down-sample these test images. Hence, we intentionally dropped three fourths of the data from the original image. The resultant down-sampled images were then used as inputs for the proposed algorithm which up-sampled them to their original size. These up-sampled images are then compared with the original images. We also up-sampled the same image using the bilinear and bicubic interpolation methods, to use for comparison with our results.

#### *A. Image Quality Metrics*

Peak signal-to-noise ratio (PSNR) and CIELAB  $\Delta E_{ab}^*$  [19], are two commonly used “quality metrics” or measures used to objectively evaluate the quality of our up-sampled images,

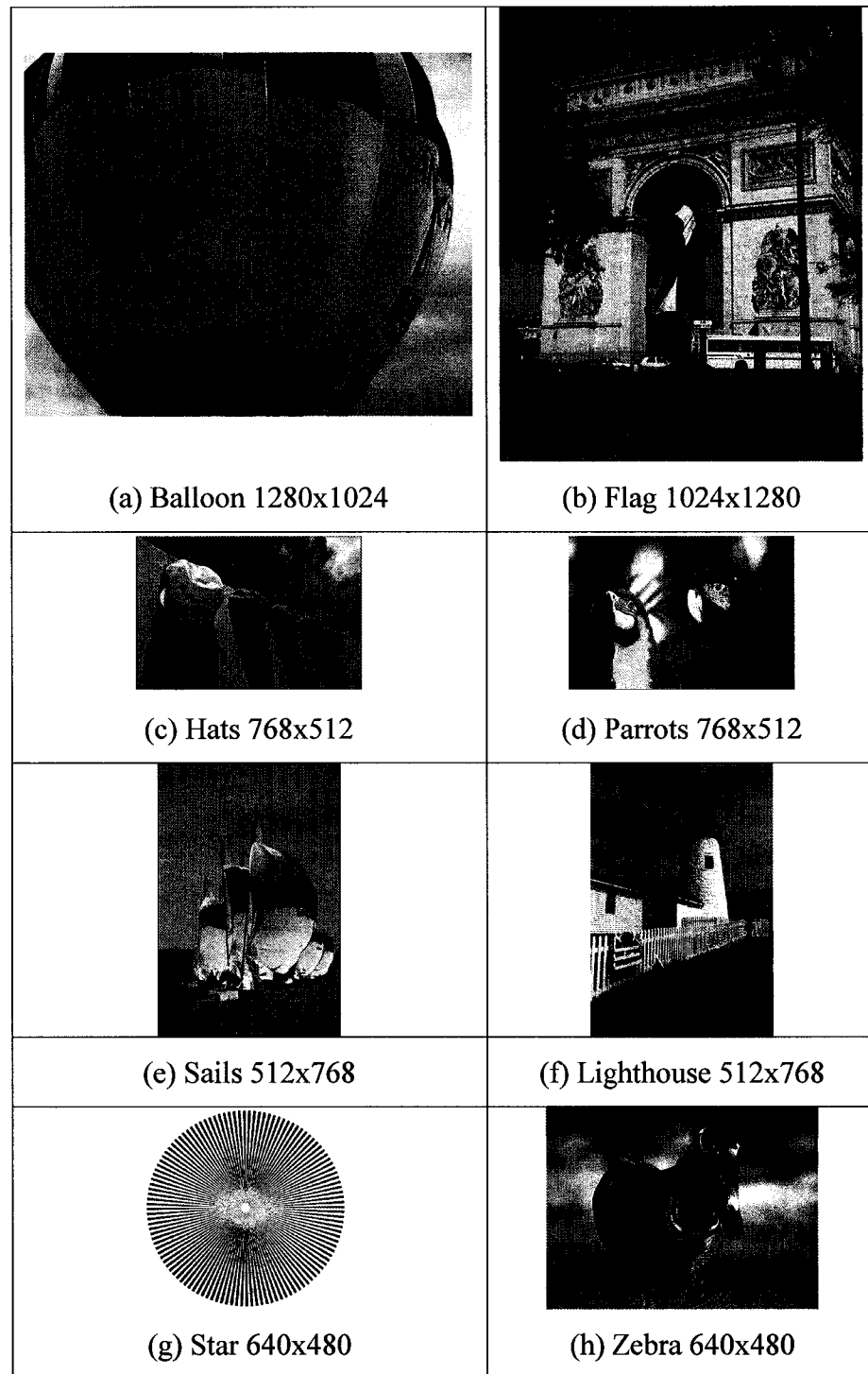


Figure 6: Original test Images used in the experiment.

or any processed image in general. The peak signal-to-noise ratio depends on another quantity known as the root-mean-squared-error (RMSE). For an image  $I$  of size  $m \times n$ , with processed or reconstructed image denoted by  $I'$ , the RMSE is given by

$$RMSE = \sqrt{\frac{1}{mn} \sum_{i=1}^m \sum_{j=1}^n [I(i, j) - I'(i, j)]^2},$$

where  $I(i, j)$  and  $I'(i, j)$  represent the gray level intensity or color value of pixel  $(i, j)$  in a given color plane of the original and processed images respectively.

For an 8 bit image, with a maximum pixel value of 255, in decibel (dB) the peak signal-to-noise ratio is given by

$$PSNR = 10 \log_{10} \left[ \frac{255^2}{RMSE^2} \right].$$

PSNR values of 40 or greater indicate that the images being compared are perceptually indistinguishable. To obtain the PSNR for a color plane of a processed image, we simply apply the formula above for the color value of a given image pixel in the color plane instead of the gray-level value. We want to emphasize that a higher PSNR value does not always imply a higher image quality. It turns out that objective quality metrics do not always correlate closely with the subjective quality of the image. However, they provide a general idea about the global image quality.

The CIELAB color scale was developed in 1976 by the Commission Internationale de l'Eclairage (luminosity) or CIE to provide a standard uniform color scale. The CIELAB metric is a “perceptual color fidelity metric” and is a measure of how close to the original color is the reproduction of the actual color according to the human eye. Color perception is dependent on spatial frequency and viewing conditions. CIELAB is a three

dimensional color space used to represent the perception of color stimuli. It is uniform because equal distances on this scale correspond to approximately equal difference in color perception. The three coordinates in this space are designated as  $L^*$ ,  $a^*$ , and  $b^*$ . The  $L^*$  axis is also known as lightness (related to luminance value) and ranges from 0 (black) to 100 (white). The difference between green ( $-a^*$ ) and red ( $+a^*$ ) is denoted as  $a^*$  and  $b^*$  represents the difference between yellow ( $+b^*$ ) and blue ( $-b^*$ ). These two parameters are related to the chromaticity and hue values.

The coordinates in the CIELAB space can be obtained from transformation of coordinates in the CIEXYZ or “tristimulus scale”, also an absolute color space. The nonlinear transformations correspond to the nonlinear (log) response of the human eye to color. The transformation formula also involves normalization factors for white light, used as the reference. The “XYZ” coordinates on the tristimulus scale are related to the spectral power sensitivities of the three types of cones found in the human retina.

Any color in the CIELAB space can be represented as a point on its associated graph.  $\Delta E^*$ , the Euclidean distance between two points in this color space is given by  $\Delta E^* = \sqrt{\Delta L^{*2} + \Delta a^{*2} + \Delta b^{*2}}$  and represents the magnitude of the difference between two color stimuli in appropriate perceptual units [20]. It is also referred to as the “total color difference.” If  $a^*$  and  $b^*$  are zero, then the  $L^*$  axis represents an achromatic range of gray levels. The delta represents the difference in scale of the sample from the standard and is used for quality control purposes.

Two points that coincide on the color plane represent the same color perception, and the greater the distance between two color points in the space, the greater the sensed color

difference. The CIELAB  $\Delta E_{ab}^*$  measures the Euclidean distance between the original and processed image in CIELAB color space. The expression for CIELAB  $\Delta E_{ab}^*$  is given by

$$\Delta E_{ab}^* = \frac{1}{mn} \sum_{i=1}^m \sum_{j=1}^n \|I(i, j)_{Lab} - I'(i, j)_{Lab}\|$$

where  $I(i, j)_{Lab}$  and  $I'(i, j)_{Lab}$  represent the CIELAB color values of pixel  $(i, j)$  in the original and processed images, and  $\|\cdot\|$  denotes L2-Norm. As discussed in [21], a value of 2.3 on this scale distinguishes the threshold for sensing a difference in color.

To convert an image from RGB color space to CIELAB color space, we first convert from the RGB scale to the CIEXYZ or tristimulus scale and then from CIEXYZ to CIELAB. The conversion matrices and formulas are provided as follows:

#### **RGB $\Leftrightarrow$ CIE XYZ (ITU D65)**

$$\begin{bmatrix} X \\ Y \\ Z \end{bmatrix} = \begin{bmatrix} 0.431 & 0.342 & 0.178 \\ 0.222 & 0.707 & 0.071 \\ 0.020 & 0.130 & 0.939 \end{bmatrix} \times \begin{bmatrix} R \\ G \\ B \end{bmatrix}$$

$$\begin{bmatrix} R \\ G \\ B \end{bmatrix} = \begin{bmatrix} 3.063 & -1.393 & -0.476 \\ -0.969 & 1.876 & 0.042 \\ 0.068 & -0.229 & 1.069 \end{bmatrix} \times \begin{bmatrix} X \\ Y \\ Z \end{bmatrix}$$

**D65** refers to the class of illuminant that resembles the relative spectral energy distribution of northern hemisphere daylight. **ITU D65** is the standard most monitors conform to.

#### **CIE XYZ $\Leftrightarrow$ CIELAB**

$$\begin{aligned}
L^* &= 116 \times f(Y/Y_n) - 16 \\
a^* &= 500 \times (f(X/X_n) - f(Y/Y_n)) \\
b^* &= 200 \times (f(Y/Y_n) - f(Z/Z_n))
\end{aligned}$$

$$f(q) = \begin{cases} q^{1/3} & \text{if } q > 0.008856 \\ 7.787 \times q + 16/116 & \text{otherwise} \end{cases}$$

$$X_n = 0.950449, Y_n = 1, Z_n = 1.0889166$$

Here, the RGB is normalized within  $[0 - 1]$ , and  $(X_n, Y_n, Z_n)$  is the white point which means  $Y=1$  and  $R=G=B$ . For more information on converting an image from RGB color space to CIELAB color space, the reader may refer to [19] and [22].

### *B. Results Using Different DWT Implementations and Filters*

In order to verify the proposed DWT based up-sampling method, we implemented two different discrete wavelet transforms – traditional filtering/convolution based implementation with Daubechies 9/7 bi-orthogonal Spline filters [7] and lifting based implementation [17, 18] with 5/3 integer filters. For the filtering based implementation, we also normalized the 9/7 filters with both DC and Nyquist gains equal to  $\sqrt{2}$ . Consequently, the scaling factor,  $s$ , used in the proposed algorithm should be 2. As for the lifting based implementation, the 5/3 filter has a DC gain of 1, so the scaling factor is set equal to 1 too.

Fig. 7 and Fig. 8 show the up-sampling images using the proposed DWT based method with the two different DWT implementations. As we can see in Fig. 9, the DWT based

up-sampled Zebra images, Fig. 9 (d - e), have much better visual quality with sharper edges as compared to the bilinear and bicubic interpolation results. We observed similar behavior with many other challenging images, such as the Star image shown in Fig. 10, as well.

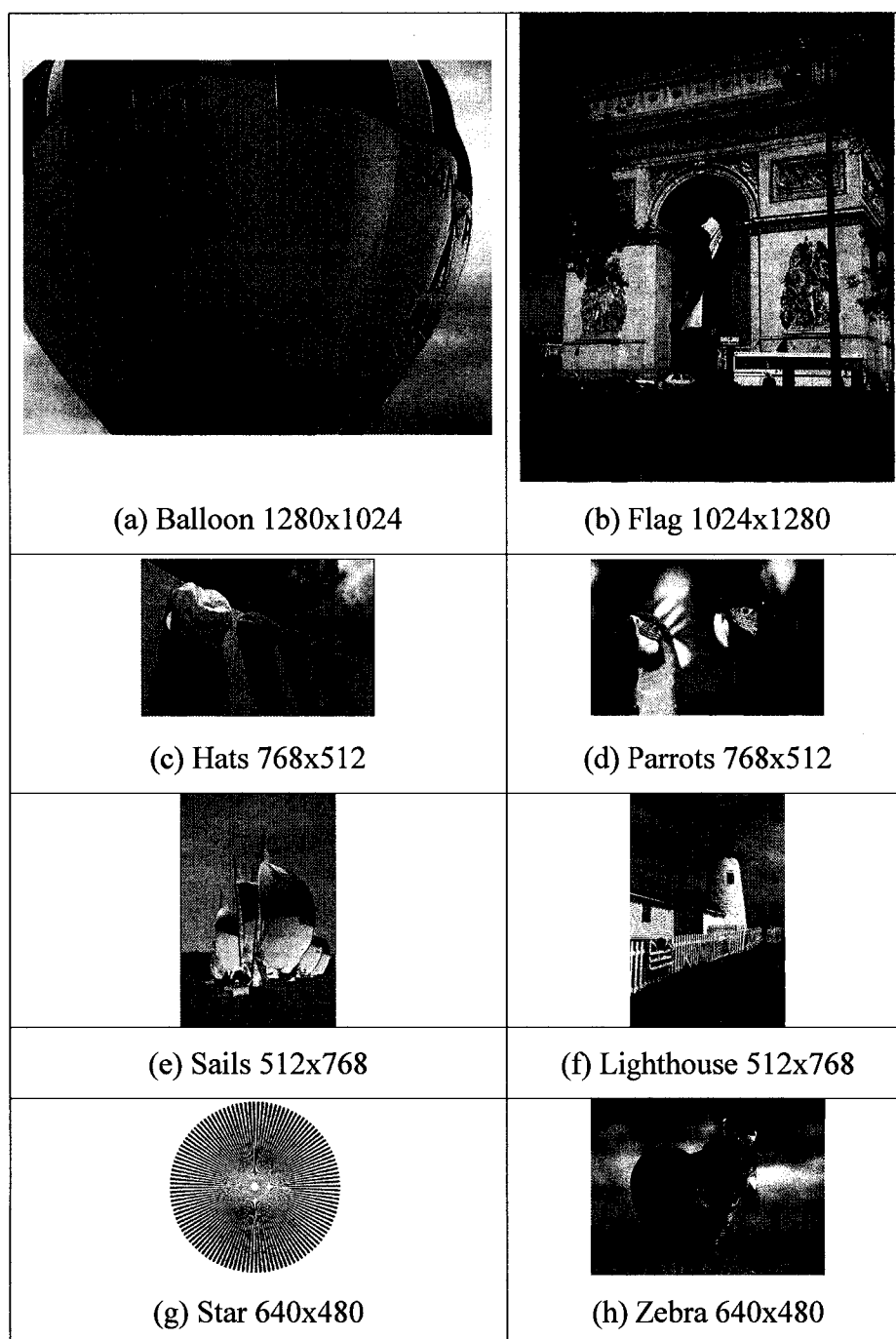


Figure 7: Up-sampling results with proposed DWT based approach using 9/7 filters.

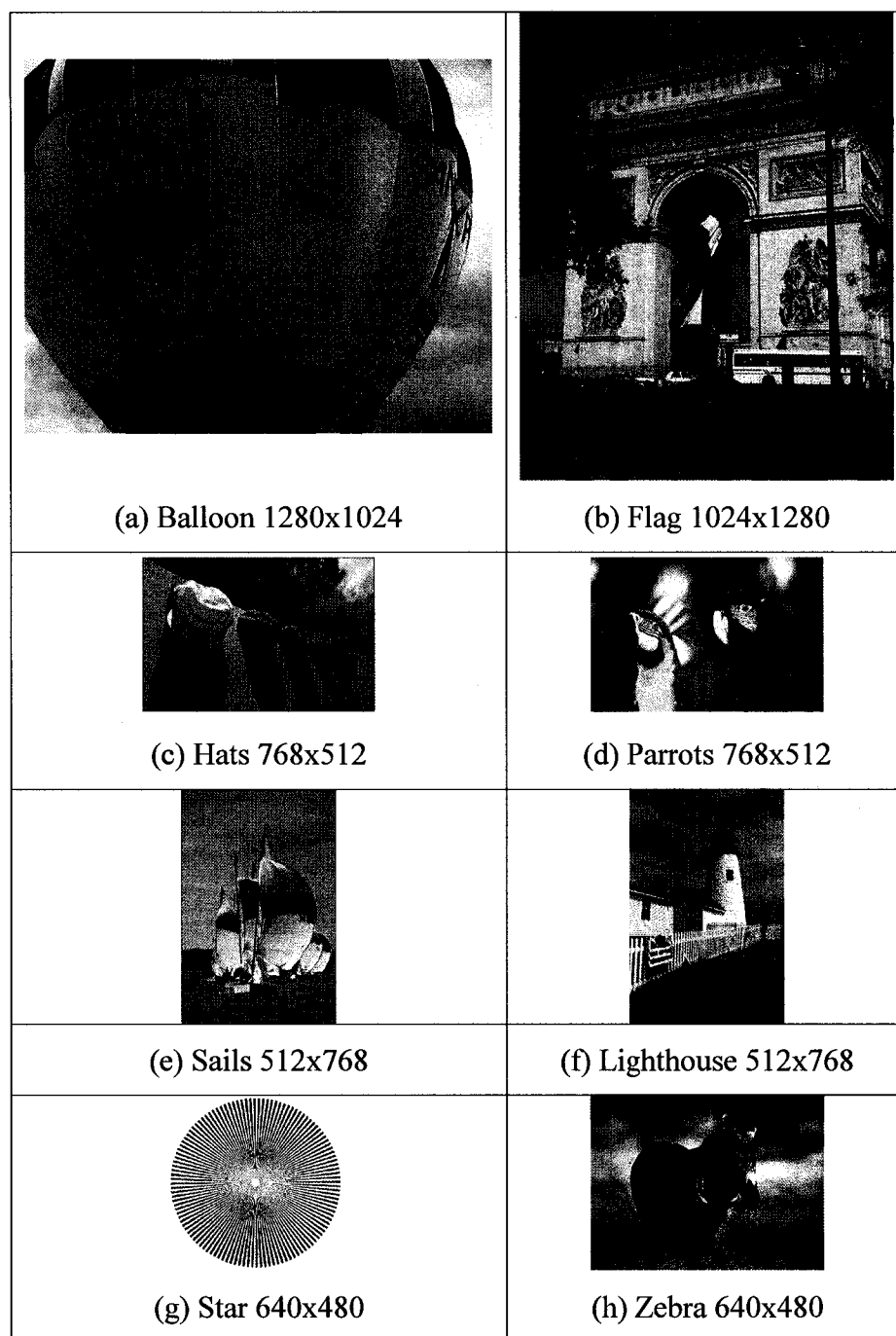


Figure 8: Up-sampling results with proposed DWT based approach using 5/3 filters.

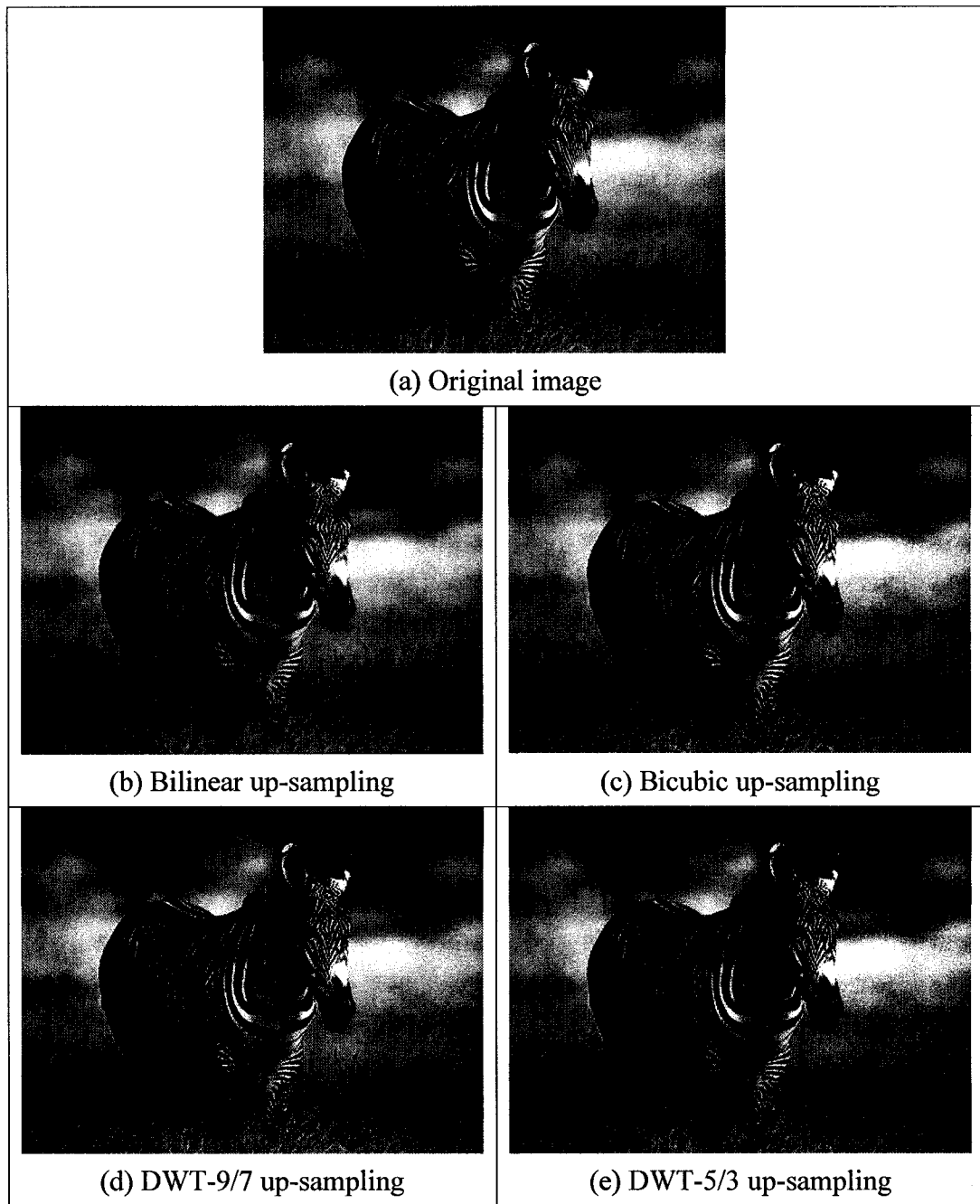


Figure 9: Experimental results for ZEBRA image.

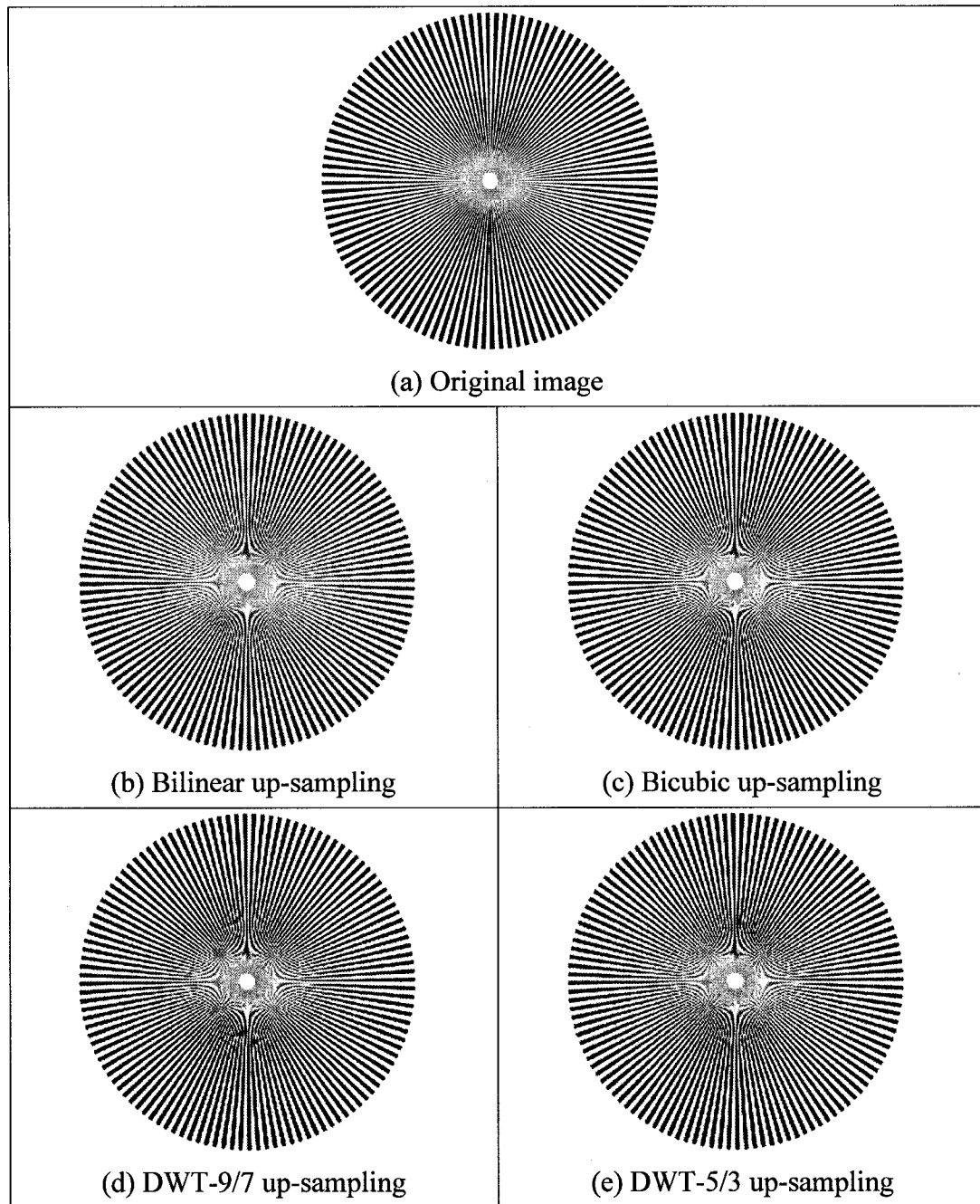


Figure 10: Experimental results for STAR image.

Table I shows the PSNR and  $\Delta E_{ab}^*$  comparisons between the proposed DWT based up-sampling (9/7 and 5/3), bilinear, and bicubic interpolation techniques. It is evident from Table I that the proposed method outperforms the bilinear and bicubic interpolations in all cases. The four nature images from Kodak Photo CD (Hat, Parrots, Sails and Lighthouse) have more compatible results between the three different up-sampling methods due to the fact that there is less sharp edge content in those images.

Table I: PSNR AND  $\Delta E_{ab}^*$  COMPARISONS

		PSNR (dB)			$\Delta E_{ab}^*$
		R	G	B	
Balloon	BL	30.14	30.22	33.14	2.67
	BC	30.09	30.29	33.05	2.70
	DWT-9/7	32.07	33.02	34.53	2.27
	DWT-5/3	<b>32.93</b>	<b>33.27</b>	<b>34.92</b>	<b>2.03</b>
Flag	BL	26.95	26.68	26.70	2.27
	BC	26.83	26.56	26.59	2.33
	DWT-9/7	28.11	27.88	28.04	2.07
	DWT-5/3	<b>28.23</b>	<b>28.00</b>	<b>28.15</b>	<b>1.86</b>
Hats	BL	30.05	30.04	30.38	1.56
	BC	29.91	29.86	30.06	1.65
	DWT-9/7	30.07	29.97	29.89	1.62
	DWT-5/3	<b>30.25</b>	<b>30.31</b>	<b>30.42</b>	<b>1.44</b>
Parrots	BL	29.96	29.95	30.83	1.51
	BC	29.91	29.92	30.74	1.58
	DWT-9/7	30.63	30.60	31.68	1.42
	DWT-5/3	<b>30.63</b>	<b>30.61</b>	<b>31.74</b>	<b>1.24</b>
Sails	BL	28.26	28.09	28.52	1.59
	BC	28.10	27.98	28.34	1.66
	DWT-9/7	28.87	<b>28.80</b>	28.93	1.55
	DWT-5/3	<b>28.87</b>	28.65	<b>28.98</b>	<b>1.41</b>
Lighthouse	BL	25.26	25.30	25.67	2.43
	BC	24.99	24.98	25.31	2.56
	DWT-9/7	25.38	25.25	25.48	2.52
	DWT-5/3	<b>25.63</b>	<b>25.55</b>	<b>25.76</b>	<b>2.18</b>
Star	BL	18.15	17.67	18.23	4.68
	BC	18.19	17.72	18.28	4.72
	DWT-9/7	<b>20.27</b>	<b>19.98</b>	<b>20.42</b>	4.17
	DWT-5/3	19.79	19.40	19.92	<b>3.81</b>
Zebra	BL	22.87	22.89	22.92	3.26
	BC	22.60	22.63	22.63	3.61
	DWT-9/7	<b>24.15</b>	<b>24.17</b>	24.06	3.38
	DWT-5/3	24.09	24.12	<b>24.19</b>	<b>2.86</b>

### C. Results for Image Fidelity

The homogeneity of an image is a measure of its uniformity and is related to the local information content around a given region of the image. It is defined in [23] as being composed of two quantities: standard deviation and discontinuity of the intensities. Standard deviation describes the contrast within a local region. Discontinuity is obtained by applying edge detectors to a given region and is a measure of its abrupt change in gray level. For a given pixel at image location  $(i, j)$ , its standard deviation is denoted as  $v(i, j)$  and its discontinuity is denoted as  $e(i, j)$ . These values are normalized for computational consistency, and the normalized standard deviation and discontinuity values for a given image location are denoted as  $V(i, j)$  and  $E(i, j)$  respectively. The homogeneity is thus given by:

$$H(i, j) = 1 - V(i, j) \times E(i, j)$$

The homogeneity value for a given image location ranges from 0 to 1, and the larger the homogeneity value at a given point, the more uniform the local region around that pixel.

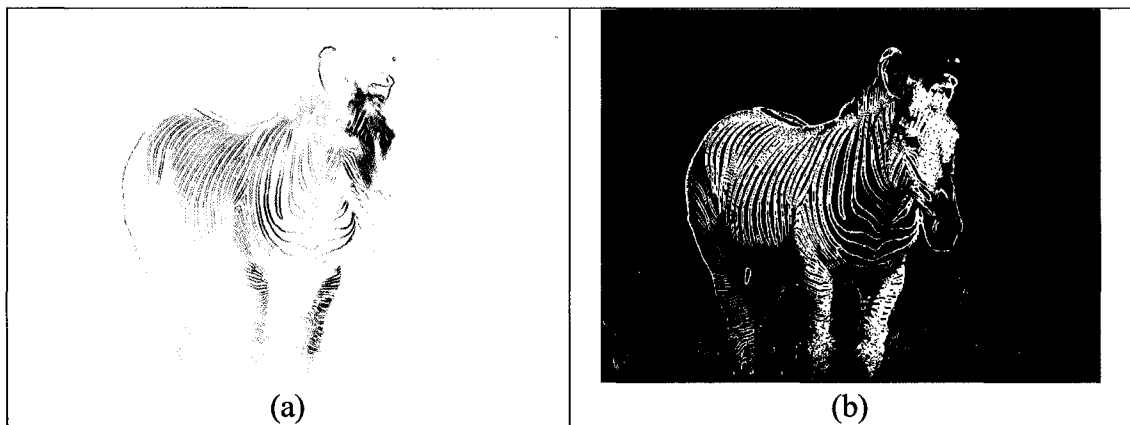


Figure 11: (a) Homogeneity image of ZEBRA green channel. (b) Blended mask image of RGB channels.

For the purpose of measuring the image fidelity, we generated a binary mask based on the homogeneity of the image. A threshold is applied to the homogeneity image, and a binary mask is generated to separate the “edge” and “smooth” regions of the image. To perform the PSNR comparisons we used a different mask for each color channel, but for the  $\Delta E_{ab}^*$  comparison, we blended the masks used for the three colors, and used a single “blended” mask in our study. As an example, we provided the homogeneity image corresponding to one of our test images – the Zebra above. Fig. 11 (a) shows the homogeneity image corresponding to the green channel of the ZEBRA image, and Fig. 11 (b) shows the blended mask image of the RGB channels. We then used the mask to compute two distinct PSNR and  $\Delta E_{ab}^*$  values: one comparing the “edge” region of the up-sampled image to the original image, and the other comparing the “smooth” region of the up-sampled image to the original image respectively. This was done since sometimes the overall PSNR and  $\Delta E_{ab}^*$  values of the entire image do not give sufficient information about different amounts and types of artifacts found around image features. A similar approach using the edge map instead of the homogeneity mask has been reported in [24].

Table II: IMAGE FIDELITY COMPARISON RESULTS

		PSNR(dB)						$\Delta E_{ab}^*$	
		R		G		B			
		Smooth	Edge	Smooth	Edge	Smooth	Edge	Smooth	Edge
Balloon	BL	38.35	20.37	40.23	19.86	39.03	23.40	1.79	9.76
	BC	38.14	20.33	40.13	19.94	38.98	23.28	1.80	9.94
	DWT 9/7	37.94	22.82	39.42	23.27	39.28	25.20	1.71	6.75
	DWT 5/3	38.72	<b>23.70</b>	40.10	<b>23.41</b>	39.57	<b>25.64</b>	1.47	<b>6.50</b>
Flag	BL	31.74	21.35	31.58	20.97	31.91	20.90	1.50	4.95
	BC	31.82	21.16	31.67	20.78	32.03	20.72	1.54	5.11
	DWT 9/7	31.49	<b>23.15</b>	31.33	<b>22.82</b>	31.69	<b>22.88</b>	1.53	3.98
	DWT 5/3	32.22	22.96	32.07	22.63	32.41	22.70	1.31	<b>3.77</b>
Hats	BL	31.91	22.84	31.85	22.71	32.08	24.20	1.21	4.46
	BC	31.71	22.80	31.60	22.64	31.73	23.99	1.27	4.69
	DWT 9/7	31.34	<b>23.96</b>	31.19	<b>23.80</b>	31.20	<b>24.40</b>	1.31	4.11
	DWT 5/3	31.79	23.57	31.87	23.43	32.18	24.12	1.13	<b>3.89</b>
Sails	BL	31.30	20.12	31.14	19.78	31.19	20.31	1.18	5.56
	BC	31.16	19.95	31.06	19.63	31.05	20.09	1.23	5.88
	DWT 9/7	31.01	<b>21.66</b>	30.93	<b>21.43</b>	30.94	<b>21.51</b>	1.22	4.74
	DWT 5/3	31.24	21.40	31.01	21.01	31.15	21.35	1.09	<b>4.49</b>
Light-house	BL	29.85	18.23	29.75	18.11	30.07	18.55	1.77	6.26
	BC	29.49	17.99	29.32	17.85	29.56	18.27	1.89	6.48
	DWT 9/7	29.10	<b>18.78</b>	28.80	18.55	28.99	<b>18.84</b>	1.93	5.92
	DWT 5/3	29.83	18.76	29.60	<b>18.56</b>	29.83	18.81	1.65	<b>5.28</b>
Parrots	BL	32.18	20.78	32.41	20.25	34.41	20.21	1.26	4.83
	BC	32.13	20.74	32.39	20.21	34.29	20.15	1.32	5.00
	DWT 9/7	32.18	<b>22.54</b>	32.44	<b>21.75</b>	34.36	<b>21.84</b>	1.23	3.85
	DWT 5/3	32.33	22.25	32.59	21.55	34.72	21.61	1.07	<b>3.53</b>
Star	BL	27.06	14.83	26.62	13.93	26.91	14.53	0.82	10.42
	BC	27.32	14.40	26.87	13.96	27.17	14.57	1.00	10.23
	DWT 9/7	26.41	<b>16.85</b>	26.19	<b>16.58</b>	26.32	<b>17.09</b>	1.34	8.36
	DWT 5/3	27.39	16.15	27.05	15.79	27.30	16.36	0.91	<b>8.12</b>
Zebra	BL	29.10	15.51	29.05	15.39	29.20	15.40	1.80	11.37
	BC	29.03	15.18	29.03	15.97	29.14	15.04	2.10	12.00
	DWT 9/7	29.29	<b>17.11</b>	29.33	<b>16.98</b>	29.10	<b>16.91</b>	2.19	9.96
	DWT 5/3	29.92	16.84	29.90	16.73	29.83	16.84	1.71	<b>9.21</b>

Table II shows the image fidelity comparison results. We obtained comparable or slightly better numbers in the smooth region of all test images, and considerably better numbers (up to 3 dB in PSNR and less than 3 units in  $\Delta E_{ab}^*$ ) for the edge region of the images when we compared DWT based up-sampling with the bilinear and bicubic

interpolation methods as expected. As before, the improvement in values in more pronounced in the images with more edge content and features. Also, we notice that our DWT 5/3 based up-sampling yields better results than the DWT 9/7 based up-sampling.

#### *D. Results for Recursive Up-sampling*

The key disadvantage of the proposed DWT based up-sampling method is that it only can up-sample the image by a factor of 2 in both horizontal and vertical directions. Compare this to the traditional bilinear or bicubic interpolation methods, which can up-sample to any size as required. In order to up-sample an image by a factor of 4 in both horizontal vertical directions, the proposed method needs to recursively apply the up-sampling method, i.e., it needs to up-sample the image by a factor of 2 in both horizontal and vertical directions twice. To evaluate the performance of recursive up-sampling, we further down sampled the two large-sized test images (Balloon and Flag) to one sixteenth of their original size. The resultant down-sampled images were then up-sampled to their original size using recursive up-sampling with DWT, bilinear, and bicubic interpolations in two steps, as compared with directly up-sampling them using bilinear and bicubic interpolations in one step. Fig. 12 shows the resultant up-sampled images using the proposed DWT-9/7 based method, and PSNR and  $\Delta E_{ab}^*$  measures for comparison. As we can see in Fig. 12, the proposed DWT based up-sampled images still outperform the bilinear/bicubic based up-sampled images in term of both PSNR and  $\Delta E_{ab}^*$  measures.

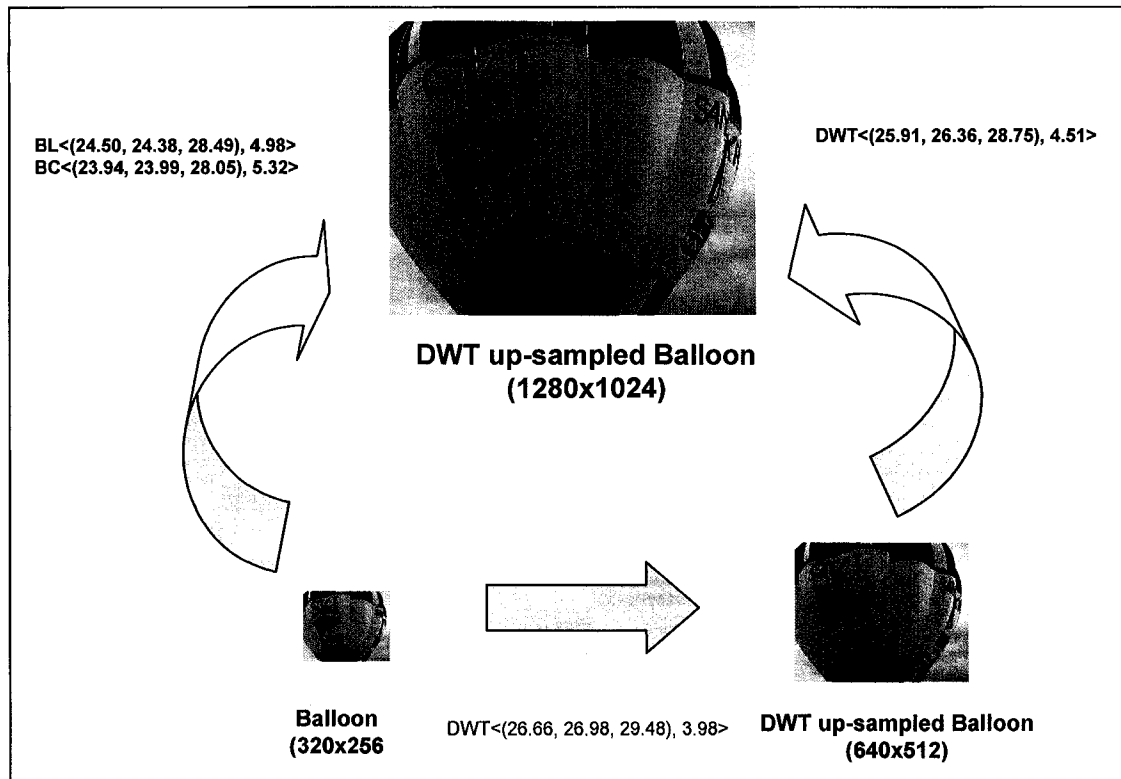


Figure 12. Experimental results for recursive up-sampling.

#### *E. Results for Combination of Bicubic and DWT*

We also tried to get around another limitation of our DWT based up-sampling, namely, that you can only multiply the image size by a power-of-two number in the horizontal and vertical directions. It turns out that we can actually expand our image to any desired size to yield any multiple of the image size in each dimension. For example, to triple our image size, we first used DWT up-sampling to double the size of the original image and then used bicubic up-sampling to multiply the resultant image by a factor of 1.5, with the end result of multiplying the image size by a factor of 3 in both horizontal and vertical directions. Basically, we like to up-sample the image, as far as possible,

using the DWT based method. Then, we up-sample the image to the desired size using the bilinear or bicubic interpolation. In terms of image quality metrics, the performance was more or less on par with up-sampling the image using the bilinear or bicubic interpolation. The DWT-based up-sampling PSNR numbers resulting from multiplying the image by a factor of 3 were in the same range as the ones obtained using the bilinear and bicubic up-sampling methods for multiplication by a factor of 3. The PSNR results of two test images are summarized in the Table III.

Table III: PSNR COMPARISONS FOR IMAGE MULTIPLIED BY A FACTOR OF THREE

		PSNR(dB)		
		R	G	B
Balloon	BL	29.60	29.81	32.43
	BC	30.43	30.74	32.94
	DWT 9/7 + BC	29.73	29.90	32.59
Flag	BL	25.64	25.38	25.50
	BC	26.26	26.03	26.18
	DWT 9/7 + BC	25.75	25.49	25.55

## CHAPTER IV

### CONCLUSION

In this thesis, we proposed an interesting image interpolation algorithm for up-scaling the resolution in an image based on the Discrete Wavelet Transform. The proposed method can be adapted for use with any wavelet filter despite their different implementation techniques. It can be easily implemented in any DWT based hardware architecture using a DSP (Digital Signal Processor). We have tested the algorithm with a large number of images of different types and sizes. We obtained better results with the images that have greater edge content and richer detail.

The proposed algorithm is suitable for up-sampling the image by a factor of 2, a power of 2, i.e. recursive multiplication by a factor of 2, or any odd or even multiple of the image dimensions without a degradation of quality. In fact the image quality as measured by the analytical metrics, as well as overall subjective quality, is higher compared to the standard image up-sampling interpolation techniques, like the bilinear and bicubic methods in the case of multiplication of the image dimensions, by any power of 2. The image quality is also much improved in the edge regions obtained from the homogeneity or uniformity measure of the image, which contains most of the image edge and feature information.

In the case of multiplication of the image dimensions by an odd factor, the quality is

on par with the standard techniques. The algorithm is suitable for interpolation of both color and gray level images. The experimental results establish that the proposed algorithm yields much better visual quality as compared to the current state-of-the-art in the literature.

## REFERENCES

- [1] S. Mallat, "A Theory for Multi-resolution Signal Decomposition: The Wavelet Representation," *IEEE Trans. on Pattern Analysis and Machine Intelligence*, vol. 11, no. 7, pp. 674-693, July 1989.
- [2] T. Acharya and A. K. Ray, *Image Processing: Principles and Applications*, John Wiley & Sons, Inc., Hoboken, NJ, 2005.
- [3] T. Acharya and P.-S. Tsai, *JPEG2000 Standard for Image Compression: Concepts, Algorithms, and VLSI Architectures*, John Wiley & Sons, Inc., NJ, 2005.
- [4] T. Acharya and P.-S. Tsai, "Edge enhanced image up-sampling algorithm using discrete wavelet transform," U.S. patent 6,377,280, Apr. 23, 2002.
- [5] R. C. Gonzalez and R. R. Woods, *Digital Image Processing*, 2/E, Prentice-Hall, Upper Saddle River, NJ, 2002.
- [6] J. D. Foley, A. van Dam, S. K. Feiner, and J. F. Hughes, *Computer Graphics: Principles and Practice*, 2/E in C, Addison-Wesley, 1997.
- [7] I. Daubechies, "The Wavelet Transform, Time-Frequency Localization and Signal Analysis," *IEEE Trans. on Information Theory*, vol. 36, no. 5, pp. 961-1005, Sept. 1990.
- [8] R. M. Rao and A. S. Bopardikar, *Wavelet Transforms: Introduction to Theory and Applications*. Addison-Wesley, MA, 1998.
- [9] Adobe® CS2 software.(<http://www.adobe.com/products/photoshop/>)

- [10] K. P. Hong, J. K. Paik, H. J. Kim, and C. H. Lee, "An Edge-Preserving Image Interpolation System for a Digital Camcorder," *IEEE Trans. on Consumer Electronics*, vol. 42, no. 3, pp. 279-284, August 1996.
- [11] X. Li and M. T. Orchard, "New Edge-Directed Interpolation," *IEEE Trans. on Image Processing*, vol. 10, no. 10, pp. 1521-1527, October 2001.
- [12] J. W. Hwang and H. S. Lee, "Adaptive Image Interpolation Based on Local Gradient Features," *IEEE Signal Processing Letters*, vol. 11, no. 3, pp. 359-362, March 2004.
- [13] S. Carrato and L. Tenze, "A High Quality  $2\times$  Image Interpolator," *IEEE Signal Processing Letter*, vol. 7, no. 6, pp. 132-134, June 2000.
- [14] M. Rabbani and D. Santa-Cruz, "The JPEG 2000 Still-Image Compression Standard," course notes given at the 2001 International Conference in Image Processing (ICIP), Thessaloniki, Greece, October 11, 2001. ([http://jj2000.epfl.ch/jj\\_publications/index.html](http://jj2000.epfl.ch/jj_publications/index.html))
- [15] D. S. Taubman and M. W. Marcellin, *JPEG2000: Image Compression Fundamentals, Standards and Practice*, Kluwer Academic Publishers, MA, 2002.
- [16] <http://r0k.us/graphics/kodak/>.
- [17] W. Sweldens, "The Lifting Scheme: A Custom-Design Construction of Bi-Orthogonal Wavelets," *Applied and Computational Harmonic Analysis*, vol. 3, no. 15, pp. 186-200, 1996.
- [18] I. Daubechies and W. Sweldens, "Factoring Wavelet Transforms Into Lifting Schemes," *The Journal of Fourier Analysis and Applications*, vol. 4, pp. 247-269, 1998.

- [19] M. D. Fairchild, *Color Appearance Models*, Reading, MA: Addison Wesley, 1997.
- [20] HunterLab, “CIE  $L^*a^*b^*$  Color Scale”, Applications Note, July 1-15, 1996, Vol. 8, No. 7. ([www.hunterlab.com/appnotes/an07\\_96a.pdf](http://www.hunterlab.com/appnotes/an07_96a.pdf))
- [21] G. Sharma and H.J. Trussell, “Digital Color Imaging”, *IEEE Transactions on Image Processing*, vol. 6, no. 7, pp. 901-932, July 1997.
- [22] “Recommendations on Uniform Color Spaces, Color Difference Equations, Psychometric Color Terms,” C.I.E, Supplement no. 2 to CIE publication no. 15(E.-1 31) 1971/(TC-1.3), 1978.
- [23] H. D. Cheng and Y. Sun, “A Hierarchical Approach to Color Image Segmentation Using Homogeneity”, *IEEE Transactions on Image Processing*, vol. 9, issue 12, pp. 2071-2082, Dec. 2000.
- [24] Wenmiao Lu and Yap-Peng Tan, “Color Filter Array Demosaicking: New Method and Performance Measures”, *IEEE Transactions on Image Processing*, vol 12, no. 10, pp. 1194-1210, Oct. 2003.

## VITA

LALEH ASGHARIAN

RR 26 Box 771D  
Edinburg, TX 78541

### Education:

B.S. in Physics from UT, Austin (1983-1987)  
M.S. in Biomedical Engineering from UT, Austin (1988-1990)  
M.S. in Mathematics from UTPA (1995-1997)

### Work Experience:

2005 – 2006 Teaching Assistant, University of Texas – Pan American, Edinburg, TX  
2003 - 2005 Lecturer, Dept. of Physics & Geology, UTPA  
2001 – 2003 Lecturer, Dept. of Mathematics, UTPA  
1998 – 2001 Instructor, Dept. of Mathematics & Developmental Studies, STCC,  
McAllen, TX

### Publications:

Ping-Sing Tsai, Tinku Acharya, and Laleh Asgharian, “Image Interpolation Using the Discrete Wavelet Transform, submitted to *IEEE Transactions on Image Processing*, Aug. 14, 2006.

Abbas Asgharian and Laleh Asgharian, “Comments on Superposition and Energy Conservation for Small Amplitude Mechanical Waves”, *The American Journal of Physics*, Feb. 1988.